Analysis of Internal Quantum Efficiency and Current Injection Efficiency in III-Nitride Light-Emitting Diodes

Hongping Zhao, Guangyu Liu, Jing Zhang, Ronald A. Arif, and Nelson Tansu

***Abstract*—Current injection efficiency and internal quantum efficiency (IQE) in InGaN quantum well (QW) based light emitting diodes (LEDs) are investigated. The analysis is based on current continuity relation for drift and diffusion carrier transport across the QW-barrier systems. A self-consistent 6-band $k \cdot p$ method is used to calculate the band structure for InGaN QW structure. Carrier-photon rate equations are utilized to describe radiative and non-radiative recombination in the QW and the barrier regions, carrier transport and capture time, and thermionic emission leading to carrier leakage out of the QW. Our model indicates that the IQE in the conventional 24-Å $In_{0.28}Ga_{0.72}N$-GaN QW structure reaches its peak at low injection current density and reduces gradually with further increase in current due to the large thermionic carrier leakage. The efficiency droop phenomenon at high current density in III-nitride LEDs is thus consistent with the high-driving-current induced quenching in current injection efficiency predicted by our model. The effects of the monomolecular recombination coefficient, Auger recombination coefficient and GaN hole mobility on the current injection efficiency and IQE are studied. Structures combining InGaN QW with thin larger energy bandgap barriers such as $Al_xGa_{1-x}N$, lattice-matched $Al_xIn_{1-x}N$, and lattice-matched $Al_xIn_yGa_{1-x-y}N$ have been analyzed to improve current injection efficiency and thus minimize droop at high current injection in III-nitride LEDs. Effect of the thickness of the larger energy bandgap barriers (AlGaN, AlInN and AlInGaN) on injection efficiency and IQE are investigated. The use of thin AlGaN barriers shows slight reduction of quenching of the injection efficiency as the current density increases. The use of thin lattice-matched AlInN or AlInGaN barriers shows significant suppression of efficiency-droop in nitride LEDs.**

***Index Terms*—Current injection efficiency, efficiency droop, III-nitride, InGaN QWs, internal quantum efficiency, light-emitting diodes (LEDs).**

I. Introduction

III-NITRIDE quantum wells (QWs) based light emitting diodes (LEDs) and laser diodes (LDs) attract intense interests in the past two decades. Significant improvements of the performance of nitride based UV and visible LEDs and LDs were reported [1]–[4]. Approaches to enhance radiative efficiency based on novel QW design with enhanced optical matrix elements have been demonstrated [5]–[16]. However, c-plane InGaN based QW LEDs suffer from the reduction in efficiency at high operating current density, i.e., "efficiency droop" [17]–[31]. Up to date, the origin of this phenomenon is still controversial. Various possible explanations were proposed as the mechanism for the efficiency droop in high power nitride LEDs as follows: 1) decreased carrier localization at In-rich regions at high injection densities [1]; 2) carrier leakage [17]–[23]; 3) hole transport impediment and consequent electron leakage [24], [25]; 4) large Auger recombination at high carrier density [27]–[31]; and 5) junction heating [32]. Approaches including the use of polarization matched AlGaInN barrier [18], [33], the novel designs of thick barriers and electron blocking layers [34]–[38] as well as the insertion of thin large bandgap materials as thin barriers [20], [39] were investigated to suppress the polarization field effects, reduce the carrier overflow, modify the current distribution across the whole active region. Specifically, the employment of thin layer of large bandgap material has been reported to have the potential of carrier leakage suppression and thus enhancement of IQE at high current density [20], [39]. Both theoretical analysis using analytical model [20] and the numerical simulation carried out in device level with the consideration of carrier transport effect [39] have shown that the lattice-matched AlInN is the optimal material candidate for this thin barrier layer attributed to largest bandgap material available with lattice-matching to GaN.

In this paper, the current injection efficiency ($\eta_{Injection}$) and internal quantum efficiency (η_{IQE}) of InGaN QW structures have been studied. Attributing to the electrostatic field in the InGaN QW, the band bending of the band edge potential leads to the thermionic escape of carriers from InGaN QW active region to the GaN barrier regions. The major contribution of the carrier leakage is from the electron leakage, due to the much higher effective mass of holes in nitride materials than that of electrons. The current injection efficiency model is based on analytical equations derived from current continuity relation for drift and diffusion carrier transport across the barrier [40]. The band structure and radiative recombination rate are calculated based on a self-consistent 6-band $k \cdot p$ method [41]–[44].

Our analysis shows that the current injection efficiency in InGaN QW reaches its peak at low current density and reduces gradually as the current density increases, which indicates that the current injection efficiency plays a crucial

Manuscript received January 11, 2013; revised February 13, 2013; accepted February 26, 2013. Date of publication March 12, 2013; date of current version March 15, 2013. This work was supported in part by the National Science Foundation (NSF) under ECCS Award 1028490, and in part by the U.S. Department of Energy under DE-FC26-08NT01581.

H. P. Zhao was with the Center for Photonics and Nanoelectronics, Department of Electrical and Computer Engineering, Lehigh University, Bethlehem, PA 18015 USA. He is currently with the Department of Electrical Engineering and Computer Science, Case Western Reserve University, Cleveland, OH 44106, USA (e-mail: hongping.zhao@case.edu)

G. Liu, J. Zhang, R. A. Arif, and N. Tansu are with the Center for Photonics and Nanoelectronics, Department of Electrical and Computer Engineering, Lehigh University, Bethlehem, PA 18015 USA (e-mail: Tansu@Lehigh.Edu).

Color versions of one or more of the figures are available online at http://ieeexplore.ieee.org.

Digital Object Identifier 10.1109/JDT.2013.2250252

role in efficiency droop for InGaN QW based LEDs. The effects of the monomolecular recombination coefficient, the Auger recombination coefficient and the GaN hole mobility on radiative efficiency ($\eta_{Radiative}$), current injection efficiency ($\eta_{Injection}$) and internal quantum efficiency (η_{IQE}) were analyzed. To suppress the efficiency droop for InGaN QW LEDs, we employed thin larger energy bandgap barrier materials (such as $Al_xGa_{1-x}N$, $Al_xIn_{1-x}N$, or $Al_xIn_yGa_{1-x-y}N$) surrounding the InGaN QW active region. The use of thin layers low-Al content AlGaN barriers sandwiched between InGaN QW and GaN barriers show slight enhancement of injection efficiency ($\eta_{Injection}$). The implementation of thin layers of lattice-matched AlInN or AlInGaN barriers sandwiched between InGaN QW and GaN barriers show significant suppression of carrier leakage, which has potential to address the efficiency droop issue in nitride LEDs. The effects of the thickness of the larger energy bandgap barriers ($Al_xGa_{1-x}N$, $Al_xIn_{1-x}N$, or $Al_xIn_yGa_{1-x-y}N$) on current injection efficiency ($\eta_{Injection}$) and internal quantum efficiency (η_{IQE}) were compared.

This paper is organized as follows: Section II introduces basic concepts related to external quantum efficiency (η_{EQE}), radiative efficiency ($\eta_{Radiative}$), current injection efficiency ($\eta_{Injection}$) and internal quantum efficiency (η_{IQE}). In Section III, the model to calculate the current injection efficiency is presented. The analysis of efficiency droop in InGaN – GaN QW structures is discussed in Section IV. The approaches to suppress the efficiency droop by employing thin larger energy bandgap barrier materials ($Al_xGa_{1-x}N$, $Al_xIn_{1-x}N$ or $Al_xIn_yGa_{1-x-y}N$) will be discussed in Section V. The use of this analytical model leads to relatively simple and physically-intuitive approach in understanding the limitation in internal quantum efficiency and droop phenomena in QW LEDs.

II. Concepts of Efficiency in Quantum Well Light-Emitting Diodes

A. External Quantum Efficiency

The external quantum efficiency (η_{EQE}) consists of the internal quantum efficiency (η_{IQE}) and light extraction efficiency ($\eta_{Extraction}$), which can be expressed as follows [40]:

$$\eta_{EQE} = \eta_{IQE} \cdot \eta_{Extraction}. \tag{1}$$

The extraction efficiency ($\eta_{Extraction}$) is defined as the ratio of the generated photon in the QW that can be extracted out from the semiconductor device to the free space. The internal quantum efficiency (η_{IQE}) is composed of two terms: the radiative efficiency ($\eta_{Radiative}$) and the current injection efficiency ($\eta_{Injection}$) as follow:

$$\eta_{IQE} = \eta_{Injection} \cdot \eta_{Radiative} \tag{2}$$

where the radiative efficiency ($\eta_{Radiative}$) is defined as the fraction of recombination current in the QW that recombines radiatively resulting in photon generation as follow:

$$\eta_{Radiative} = \frac{R_{sp}}{R_{sp} + R_{non\_rad}} \tag{3}$$

TABLE I
Energy Bandgap of Lattice-Matched $Al_xIn_yGa_{1-x-y}N$ ($x = 4.66y$) to GaN With $x = 0.1,\ 0.15, 0.2, 0.25$, and 0.3

	1	2	3	4	5
Al-content (x)	0.1	0.15	0.2	0.25	0.3
In-content (y)	0.022	0.032	0.043	0.054	0.065
E_g-$Al_xIn_yGa_{1-x-y}N$ (eV)	3.51	3.56	3.60	3.65	3.69

and the current injection efficiency ($\eta_{Injection}$) represents the fraction of the injected current that recombines both radiatively and nonradiatively in the QW active region [40].

B. Radiative Efficiency and Recombination Rates in Quantum Well

The calculation of the band structure and spontaneous emission radiative recombination rate (R_{sp}) is based on a 6-band $\boldsymbol{k}\cdot\boldsymbol{p}$ method taking into account the valence band mixing, strain effect, and spontaneous and piezoelectric polarizations as well as the carrier screening effect [44]. The details of the theoretical and numerical model were presented in [44]. The parameters for the binary GaN and InN were summarized in Table I in [44]. In (3), the nonradiative recombination term consists of the monomolecular recombination and the Auger recombination as follows:

$$R_{non\_rad} = A \cdot N + C \cdot N^3 \tag{4}$$

where A represents the monomolecular recombination coefficient and C represents the Auger recombination coefficient. The parameter N is the carrier density in QW. Note that both monomolecular recombination and Auger recombination were taken into consideration in this analysis.

C. Internal Quantum Efficiency

Both radiative efficiency ($\eta_{Radiative}$) and current injection efficiency ($\eta_{Injection}$) in InGaN QWs depend on the current injection level. Thus, in this chapter, both radiative efficiency ($\eta_{Radiative}$) and current injection efficiency ($\eta_{Injection}$) were calculated as a function of the current density. However, the extraction efficiency ($\eta_{Extraction}$) can be assumed as constant for varying injection current level. Thus, the study of the efficiency droop in external quantum efficiency (η_{EQE}) in InGaN QW corresponds to the efficiency droop in internal quantum efficiency (η_{IQE}), which includes both radiative efficiency ($\eta_{Radiative}$) and current injection efficiency ($\eta_{Injection}$).

III. Model of Current Injection Efficiency for InGaN LEDs

A. Formulation of Current Injection Efficiency Model for Quantum Well LEDs/Lasers

The formulation of current injection efficiency model for quantum well lasers/LED devices follows the treatment in [40]. In [40], the current injection efficiency model for GaAs-based laser devices was developed, and we extend the treatment of the model for GaN-based LED devices in this work. The following carrier-photon rate equations are utilized to describe the

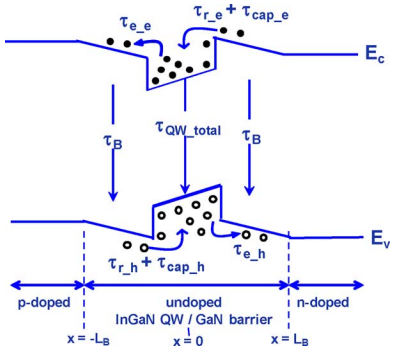

Fig. 1. Schematic of a single quantum well (QW) structure used in the numerical model. The constants representing carrier transport (τ_r), carrier capture by the QW (τ_{cap}), carrier recombination in the QW and the barrier (τ_{QW_total} and τ_B), and thermionic emission (τ_e) are shown.

quantum mechanical radiative and non-radiative recombination processes in the QW active region and the barrier regions, as well as thermionic emission leading to carrier leakage from the QW active region to the barrier regions [40]:

$$\frac{dN_{QW}}{dt} = \frac{N_B}{\tau_{bw}} \cdot \frac{V_B}{V_{QW}} - N_{QW} \cdot \left(\frac{1}{\tau_{QW\_rad}} + \frac{1}{\tau_{QW\_nonrad}} + \frac{1}{\tau_e} \right) - \frac{v_g \cdot g \cdot S}{1 + \varepsilon \cdot S} \tag{5}$$

$$\frac{dN_B}{dt} = \frac{I_{total}}{q \cdot V_B} - N_B \cdot \left(\frac{1}{\tau_B} + \frac{1}{\tau_{bw}} \right) + \frac{N_{QW}}{\tau_e} \cdot \frac{V_{QW}}{V_B} \tag{6}$$

$$\frac{dS}{dt} = \frac{\Gamma \cdot v_g \cdot g \cdot S}{1 + \varepsilon \cdot S} - \frac{S}{\tau_{ph}} + \frac{\Gamma \cdot \beta \cdot N_{QW}}{\tau_{QW\_rad}}. \tag{7}$$

For clarity, the schematic for the QW structure used in the analysis with the corresponding parameters is shown in Fig. 1. The (5) and (6) describe the dynamic of the carrier density in the QW (N_{QW}) and barrier (N_B) regions, respectively. A constant supply of injected carrier is provided by DC total injected current (I_{total}) from the n- and p-cladding layers into the barrier regions. The parameters V_B and V_{QW} are the volumes of the barrier and QW regions. The barrier-well lifetime (τ_{bw}) consists of carrier transport lifetime across the barrier (τ_r) and carrier capture lifetime by the QW (τ_{cap}) [$\tau_{bw} = \tau_r + \tau_{cap}$]. The carrier radiative lifetime (τ_{rad}) and nonradiative lifetime (τ_{no_rad}) can be obtained as follows:

$$\frac{1}{\tau_{Rad}} = \frac{R_{sp}}{N} \tag{8}$$

$$\frac{1}{\tau_{non\_rad}} = \frac{R_{non\_rad}}{N}. \tag{9}$$

Note that the carrier lifetime (τ_B) in the barrier can also be calculated in a similar manner with the respective carrier recombination constants in the barrier region. The thermionic emission lifetime τ_e is calculated following standard themionic emission theory described in [40], [45], and [46].

In (7), the dynamic relation of the photon density (S) is described. The parameters g, v_g, Γ, τ_{ph}, and β are the peak gain, group velocity of the mode, mode overlap with the active region, photon lifetime and spontaneous recombination factor, respectively. The parameter ε is the intrinsic gain compression factor. In steady state condition, the (5) and (6) can be set to be equal to zero, thus the following equation relates total injected current (I_{total}) and total recombination current in the QW (I_{QW_total}) can be expressed as

$$I_{total} = I_{QW\_total} \left\{ 1 + \frac{\tau_{bw}}{\tau_B} \cdot \left[1 + \frac{\tau_{QW\_total}}{\tau_e} + \left(1 + \frac{\tau_B}{\tau_{bw}} \right) \cdot \left(\frac{\tau_{QW\_total}}{N_{QW}} \cdot \frac{v_g \cdot g \cdot S}{1 + \varepsilon \cdot S} \right) \right] \right\}. \tag{10}$$

In the case of QW LEDs/lasers with minimum drift leakage (i.e., employing large bandgap cladding layer), the total injected current (I_{total}) is equal to the summation of both the total recombination current in the QW (I_{QW_total}) and total recombination current in the barrier regions ($I_{Barrier\_total}$). The recombination currents in both the QW and barrier layers consist of all the recombination processes in those layers.

The current injection efficiency is the fraction of current injected into the QW that recombines radiatively and non-radiatively with respect to total injected current, which can be expressed as follow:

$$\eta_{Injection} = \frac{I_{QW\_total}}{I_{total}} \tag{11}$$

Note that the parameter S corresponds to the photon density of the lasing mode. As we are considering below threshold condition for LED application, $S \approx 0$, and the parameter $\eta_{Injection}$ can then be simplified to the following relation [40]:

$$\eta_{Injection\_below\_threshold}(S \approx 0) \equiv \frac{1}{1 + \frac{\tau_{bw}}{\tau_B} \cdot \left(1 + \frac{\tau_{QW\_total}}{\tau_e} \right)}. \tag{12}$$

In the (12), the total carrier lifetime in the barrier τ_B and the total carrier lifetime in the QW region τ_{QW_total} are obtained based on the (8) and (9). Calculation of the total thermionic carrier escape lifetime τ_e and barrier-well lifetime τ_{bw} will be introduced in Sections III.B and III.C, respectively.

B. Thermionic Carrier Escape Rate for Quantum Wells—Barrier LEDs

The thermionic carrier lifetime is an important factor for the current injection efficiency ($\eta_{Injection}$) in QW structures. A large thermionic lifetime (τ_e) of the carriers in the QW indicates a minimal escape rate of the carriers from the QW to the barriers. The derivation of the thermionic carrier leakage follows the treatment presented in [40] with the following assumptions: (1) the carriers in the QW are under thermal equilibrium, (2) the net current flow does not affect this equilibrium, and (3) the barrier height is much larger than the thermal energy ($k_B T$).

The thermionic carrier leakage with the leakage of both electrons and holes from QW to one side of the barrier can be expressed as follows (electron leakage current $J_{thermionic\_e}$, and hole leakage current $J_{thermionic\_h}$) [45], [46]:

$$J_{thermionic\_e} = \frac{4\pi \cdot q \cdot (k_B T)^2}{h^3} \cdot m_e^* \cdot \exp\left(-\frac{E_{b\_e} - F_e}{k_B T} \right) \tag{13.a}$$

$$J_{thermionic\_h} = \frac{4\pi \cdot q \cdot (k_B T)^2}{h^3} \cdot m_h^* \cdot \exp\left(-\frac{E_{b\_h} - F_h}{k_B T} \right) \tag{13.b}$$

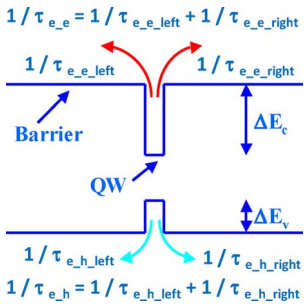

Fig. 2. Schematic of the thermionic carrier leakage processes for QW-active region.

where m_e^* (m_h^*) is the effective mass of the electron (hole) in the QW, E_{b_e} (E_{b_h}) is the effective barriers for conduction (valence) band, and F_e (F_h) represents the quasi-Fermi levels for the electrons (holes) in the QW.

The thermionic emission carrier lifetime for electrons (τ_{e_e}) and holes (τ_{e_h}) related to the thermionic current leakage can be expressed as follows [40]:

$$\tau_{e\_e} = \frac{n\ q\ L_z\ N_{QW}}{J_{thermionic\_e}} \tag{14.a}$$

$$\tau_{e\_h} = \frac{n\ q\ L_z\ N_{QW}}{J_{thermionic\_h}} \tag{14.b}$$

where n is the number of QWs, q is the charge of the electron, and L_z represents the QW thickness.

The total current leakage from the single quantum well (SQW) to both sides of the barriers as shown in Fig. 2, contributed by electrons (15.a) and holes (15.b) can be expressed as

$$J_{thermionic\_e} = J_{thermionic\_e\_left} + J_{thermionic\_e\_right} \tag{15.a}$$

$$J_{thermionic\_h} = J_{thermionic\_h\_left} + J_{thermionic\_h\_right}. \tag{15.b}$$

Thus, the thermionic emission carrier lifetime for electrons and holes can be expressed as

$$\frac{1}{\tau_{e\_e}} = \frac{1}{\tau_{e\_e\_\text{left}}} + \frac{1}{\tau_{e\_e\_\text{right}}} \tag{16.a}$$

$$\frac{1}{\tau_{e\_h}} = \frac{1}{\tau_{e\_h\_\text{left}}} + \frac{1}{\tau_{e\_h\_\text{right}}}. \tag{16.b}$$

Then, the total thermionic carrier escape time (τ_e) of QW can be expressed as functions of the thermionic escape time of electrons and holes as follows:

$$\frac{1}{\tau_e} = \frac{1}{\tau_{e\_e}} + \frac{1}{\tau_{e\_h}}. \tag{17}$$

Note that for c-plane nitride material system, the existence of the polarization field in both QW and barrier regions lead to the band bending of the band lineups as shown in Fig. 1. By comparing the thermionic carrier escape time from two sides of the barriers (left and right), $\tau_{e\_e\_\text{left}}$ is 6 orders higher than $\tau_{e\_e\_\text{right}}$, and $\tau_{e\_h\_\text{right}}$ is 7 orders higher than $\tau_{e\_h\_\text{left}}$. Thus, the total electron leakage is dominated by the electron leakage from the right side barrier, while the total hole leakage is dominated by the hole leakage from the left side barrier. The comparison of the τ_{e_e} and τ_{e_h} shows that the thermionic hole escape time is much higher than that of the electron. At low carrier density ($N_{QW} < 1\times10^{19}$ cm^{-3}), τ_{e_h} is 3–4 times higher than τ_{e_e}. At high carrier density ($N_{QW} > 1 \times 10^{19}$ cm^{-3}), τ_{e_h} is 2–3 orders higher than τ_{e_h}.

C. Barrier-Well Lifetime (τ_{bw}) in QW LEDs

The barrier-well capture time (τ_{bw}) consists of the carrier transport time (τ_r) and the quantum capture time (τ_{cap}).

$$\tau_{bw} = \tau_r + \tau_{cap}. \tag{18}$$

The quantum capture time (τ_{cap}) is typically in the femtosecond regime, and this value is much smaller than the contribution from τ_r in the τ_{bw}. The carrier transport time (τ_r) from the barrier to the QW follows the ambipolar carrier transport [27] as follows:

$$\tau_r = \frac{1}{2}\cdot\left(\frac{{L_S}^2}{2\cdot D_p} + \frac{{L_S}^2}{2\cdot D_n}\right) \tag{19}$$

where parameter L_S is the thickness of the updoped barrier region. Parameters D_p and D_n are the diffusion coefficient for electrons and holes, which can be obtained as follows:

$$D_p = \left(\frac{k_B T}{q}\right)\mu_p \tag{20.a}$$

$$D_n = \left(\frac{k_B T}{q}\right)\mu_n. \tag{20.b}$$

The parameters μ_p and μ_n represent the hole mobility and electron mobility, respectively.

D. Material Parameters of Interest

The material parameters of nitride semiconductors employed in the calculation are obtained from [47] and [48]. For the calculation of the energy band gap of InGaN/AlGaN/AlInN ternaries, bowing parameters of 1.4 eV/0.8 eV [47], [48]/4.1 eV [49] are used in the calculation. The band offset ratio of the conduction band to valence band $\Delta E_c : \Delta E_v$ for GaN/InGaN, GaN/AlGaN, and GaN/AlInN are 0.7:0.3, 0.7:0.3, and 0.62:0.38, respectively.

The GaN electron mobility value of 940 cm$^2/(\text{V}\cdot\text{s})$ at T = 300 K is used, which is obtained from [50]. The GaN hole mobility value of 22 cm$^2/(\text{V}\cdot\text{s})$ is used in the calculation [51]. The effect of the GaN hole mobility value on both injection efficiency ($\eta_{Injection}$) and internal quantum efficiency (η_{IQE}) are studied and presented in Section IV.D. The carrier capture time (τ_{cap}) from GaN barrier into InGaN QW of 700 fs is used in the calculation [52]. Note that the barrier thickness $L_S = 10$ nm was used in this calculation.

Note that values of monomolecular recombination coefficient (A) have been widely reported from the range of $A = 1 \times 10^6$ s^{-1} up to $A = 3 \times 10^8$ s^{-1} [17], [27], [53], and these discrepancies on the reported values can be attributed to the variation in material quality reported by different groups. We utilize monomolecular recombination coefficient $A = 1 \times 10^6$ s^{-1} for InGaN QW, and the corresponding barriers (GaN, AlGaN,

and AlInN layers). The effect of the monomolecular recombination coefficient (A) on current injection efficiency ($\eta_{Injection}$) and internal quantum efficiency (η_{IQE}) is investigated and presented in Section IV-B.

The Auger recombination rate in wide bandgap III-Nitride semiconductor is predicted to be significantly lower, in comparison to that of monomolecular and radiative recombination rates. Recent theoretical studies predicted Auger recombination coefficient to be $C = 3.5 \times 10^{-34}$ cm^6/s [54]. However, it is important to note that recent experimental studies have indicated the possibility that the Auger recombination coefficient in thick InGaN/GaN double heterostructure active regions ($d_{Active} = 10 - 77$ nm) in the range of $C = 1.4 \times 10^{-30}$ cm^6/s up to $C = 2 \times 10^{-30}$ cm^6/s [27]–[29]. Further studies are still required to clarify and confirm the Auger coefficients (C) for InGaN – GaN QW system, due to the large discrepancies from the reported Auger coefficients in the literatures [27]–[29], [54]. Note that the Auger recombination coefficient of $C = 3.5 \times 10^{-34}$ cm^6/s from the theoretical analysis in InGaN – GaN QW system [54] was employed in this analysis. The effect of the Auger recombination coefficient (C) on both injection efficiency ($\eta_{Injection}$) and internal quantum efficiency (η_{IQE}) is investigated and presented in Section IV-C.

E. Effective Band Offset for InGaN-GaN QW

The effective band offset parameter is an important parameter in analyzing the effective thermionic carrier escape rate. The effective band offset in InGaAs-GaAs QW, which does not have internal polarization field, can be determined from the conduction and valence band offset. In contrast to the case of InGaAs-GaAs QW heterostructure, the existence of polar InGaN-GaN QW results in asymmetric band offsets for the two sides of the QW layer ([as shown in Fig. 3(b)]. Fig. 3 shows the schematic of the band lineups for the conventional InGaN–GaN QW structure without the polarization fields [Fig. 3(a)] and with polarization fields [Fig. 3(b)]. Note that the band offsets are symmetric at the bottom and top GaN barrier sides for the case of flat band lineup as shown in Fig. 3(a). However, for the c-plane InGaN QW, the existence of the spontaneous and piezoelectric polarizations result in the band bending of the band lineups as shown in Fig. 3(b). The electrostatic filed leads to the asymmetric distribution of the electrons and holes in the QW and the tilting of the band lineups results in the leakage of electrons to the top GaN barrier and the leakage of holes to the bottom GaN barrier.

From (13.a) and (13.b), the thermionic electron leakage current density and thermionic hole leakage current density are related to the effective barrier height. The effective barrier height for electron (ΔE_{bc}) and hole (ΔE_{bh}), respectively, can be expressed as follows:

$$\Delta E_{bc} = E_{b\_e} - F_e \text{ (for electron)} \quad (21.a)$$

$$\Delta E_{bh} = E_{b\_h} - F_h \text{ (for hole)}. \quad (21.b)$$

The parameters F_e and F_h are the quasi-Fermi energy levels for conduction band and valence band, respectively. The parameters E_{b_e} and E_{b_h} correspond to the barrier edge energy level for conduction band and valence band, respectively. The definitions of these parameters are illustrated in Fig. 3(a) for the QW structure with rectangular shape. For the case of non-polar QW structure, the parameters E_{b_e} and E_{b_h} will correspond to the conduction (ΔE_c) and valence (ΔE_v) band offsets between the QW and barrier layers.

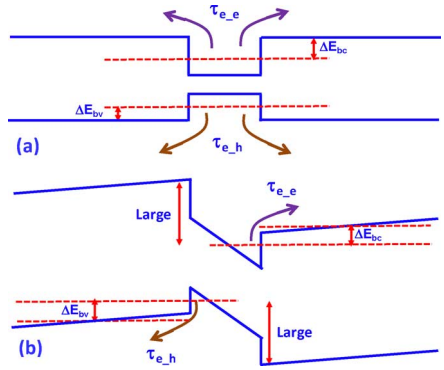

Fig. 3. Treatment of the effective barrier height for InGaN-GaN QW structure.

In the case of the polar QW-barrier system, the existence of the electric filed in III-Nitride semiconductor materials results in energy band bending in GaN barrier layer, as shown in Fig. 3(b). To take into account the asymmetric barrier height effect, the effective band edge energy levels E_{b_e} and E_{b_h} are treated as the average height of the barriers as shown in Fig. 3(b). The approximation of the effective barrier edge energy levels (E_{b_e} and E_{b_h}) in this analysis by employing the average barrier height may influence the absolute value of the current injection efficiency ($\eta_{Injection}$). However, this assumption will not change the trend and physical understanding from the results discussed by employing this model.

IV. Efficiency Droop in InGaN QW LEDs

A. Role of Injection Efficiency on Efficiency Droop in InGaN QW LEDs With GaN Barriers

The efficiency droop in InGaN – GaN QW structure was investigated. The radiaitve efficiency ($\eta_{Radiative}$), current injection efficiency ($\eta_{Injection}$) and internal quantum efficiency (η_{IQE}) were calculated for 480-nm emitting 24-Å $In_{0.28}Ga_{0.72}N$ QW LEDs with GaN barriers as a function of carrier density (N), as shown in Fig. 4(a). From the analysis, the current injection efficiency ($\eta_{Injection}$) is relatively constant up to carrier density in the range of $N = 1.5 - 2 \times 10^{19}$ cm^{-3}, however, the injection efficiency ($\eta_{Injection}$) starts to exhibit drooping phenomenon for carrier density above $N = 2 \times 10^{19}$ cm^{-3}. In contrast to that, the radiative efficiency ($\eta_{Radiative}$) exhibit monotonically increasing trend as a function of carrier density.

Fig. 4(b) shows the radiative efficiency ($\eta_{Radiative}$), current injection efficiency ($\eta_{Injection}$), and the internal quantum efficiency (η_{IQE}) as a function of the total current density (J_{tot}) for 480-nm emitting 24-Å $In_{0.28}Ga_{0.72}N$ QW LEDs with GaN barriers. The thicknesses of the upper and lower GaN barrier layers are 10-nm. Note that the monomolecular recombination coefficient A of 1×10^6 s^{-1} and Auger recombination coefficient C of 3.5×10^{-34} cm^6/s were used in the calculation. From Fig. 4(b), the radiative efficiency ($\eta_{Radiative}$) is found

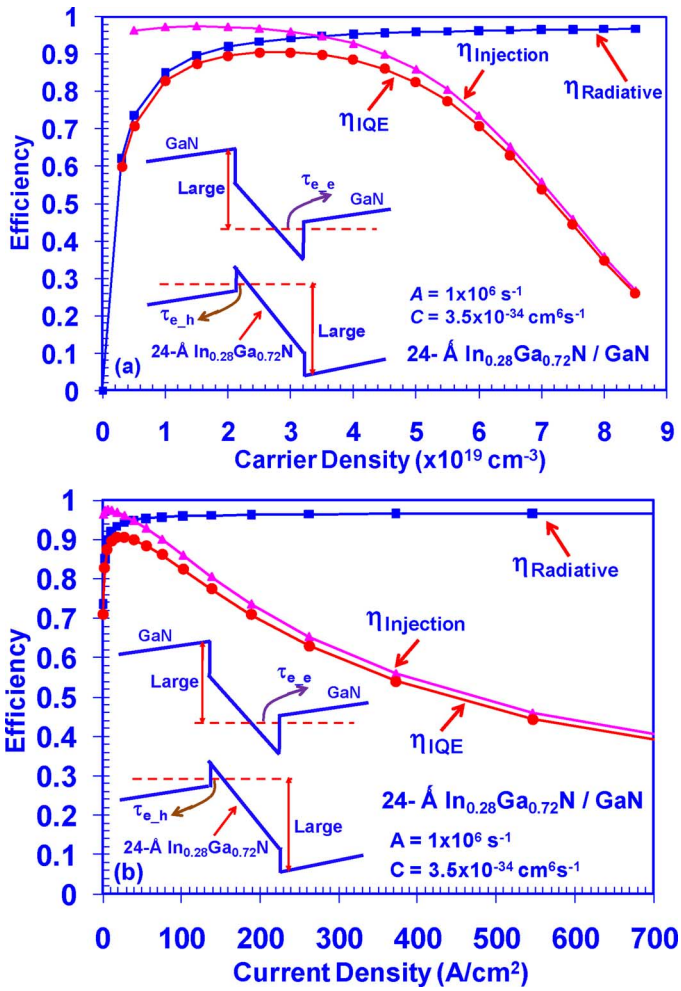

Fig. 4. IQE (η_{IQE}), radiative efficiency ($\eta_{Radiative}$) and current injection efficiency ($\eta_{Injection}$) of 24-Å $In_{0.28}Ga_{0.72}N$ QW surrounded by 10-nm GaN barrier ($\lambda = 480$ nm) at 300 K as a function of (a) carrier density and (b) total current density.

to rapidly increase at very low current density and approaches unity asymptotically at high current density. The injection efficiency ($\eta_{Injection}$) decreases significantly from almost unity with increasing current density. As a result, the internal quantum efficiency (η_{IQE}) increases rapidly at low current density and reaches its peak (at $J_{peak} \sim 10 - 20$ A/cm^2) and subsequently exhibits gradual droop with increasing current injection due to the increased carrier thermionic emission. The internal quantum efficiency (η_{IQE}) is reduced to 50% of the peak value at current density $J_{tot} \sim 550$ A/cm^2. This behavior predicted by our model is in a good agreement with the experimentally-reported efficiency-droop trends in InGaN QW LEDs [55], [56].

Based on the finding described here, the current injection efficiency needs to be taken into account in the analysis to understand the dominant factors impacting the efficiency-droop in InGaN QW LEDs. It is also important to note that analysis or measurements without taking into account the current injection efficiency or carrier leakages could potentially lead to overestimation of Auger recombination coefficient in InGaN-GaN QW heterostructure. The non-unity injection efficiency at high current density of InGaN-GaN QW LEDs has also been confirmed by some recent works [21]–[23], [39]. Specifically, the numerical simulation of InGaN-GaN QW LED by APSYS also pointed out the observation of large carrier leakage after active region at high current density [39]. Thus, the understanding of the existence of carrier leakage issue in InGaN QW LEDs operating at very high current density is important for enabling potential solutions to address the efficiency-droop in nitride LEDs.

B. Effect of the Monomolecular Recombination Process on Efficiency Droop

To investigate the effect of the monomolecular recombination coefficient (A) on the internal quantum efficiency (η_{IQE}), four different values of A (1×10^6 s^{-1}, 5×10^6 s^{-1}, 1×10^7 s^{-1} and 5×10^7 s^{-1}) were calculated. The radiative efficiency ($\eta_{Radiative}$), injection efficiency ($\eta_{Injection}$) and internal quantum efficiency (η_{IQE}) for the four cases were plotted as a function of the total current density (J_{tot}) for 24-Å $In_{0.28}Ga_{0.72}N$ QW as shown in Fig. 5(a)–(c), respectively. Note that the Auger recombination coefficient (C) of 3.5×10^{-34} cm^6/s was used in this analysis. By referring to (3) and (4), as A increases, the radiative efficiency ($\eta_{Radiative}$) decreases as shown in Fig. 5(a). Fig. 5(b) indicates that the injection efficiency ($\eta_{Injection}$) increases as A increases, which is due to the reduction of the nonradiative carrier lifetime, in turn the reduction of the total carrier lifetime (η_{QW_total}) in QW based on (12). By multiplying η Injection and $\eta_{\mathrm{Radiaitve}}$, the internal quantum efficiency (η_{IQE}) is plotted as shown in Fig. 5(c). Fig. 5(c) shows that the peak efficiency of η_{IQE} decreases as A increases, which also shifts toward higher current density (J_{peak}) as A increases.

Note that the monomolecular recombination coefficient (A) represents the material quality. Lower value of A indicates better material quality. The results shown in Fig. 5 show a good agreement between our model and reported experimental results [17]. The explanation behind the η_{IQE} behavior for different materials quality is discussed as follow. In good quality materials (small A value), the asymptotic increase of radiative efficiency $\eta_{\mathrm{Radiaitve}}$ toward unity occurs at much earlier current injection and at a higher rate, which leads to a high peak η_{IQE} at small injection current. With increasing injection current, however, the droop in η_{IQE} is subsequently dominated by current injection efficiency ($\eta_{Injection}$) quenching due to thermionic emission of carriers. In poor quality materials, the large non-radiative recombination constant suppresses the achievable peak internal quantum efficiency (η_{IQE}) at low injection current. At high injection current the internal quantum efficiency (η_{IQE}) looks flatter due to the slow asymptotic rise of the radiative efficiency ($\eta_{Radiative}$), which partially compensates the current injection efficiency ($\eta_{Injection}$) quenching.

C. Effect of Auger Recombination Process on Efficiency Droop

To investigate the effect of the Auger recombination coefficient on the internal quantum efficiency (η_{IQE}), four Auger recombination coefficient values (C) of 3.5×10^{-34} cm^6/s, 3.5×10^{-33} cm^6/s, 3.5×10^{-32} cm^6/s and 3.5×10^{-31} cm^6/s were used to calculate both radiative efficiency ($\eta_{Radiative}$) and current injection efficiency ($\eta_{Injection}$) as shown in Fig. 6(a)–(b), and Fig. 7(a)–(b), respectively. The monomolecular recombination coefficients $A = 1\times10^7$ s^{-1} and

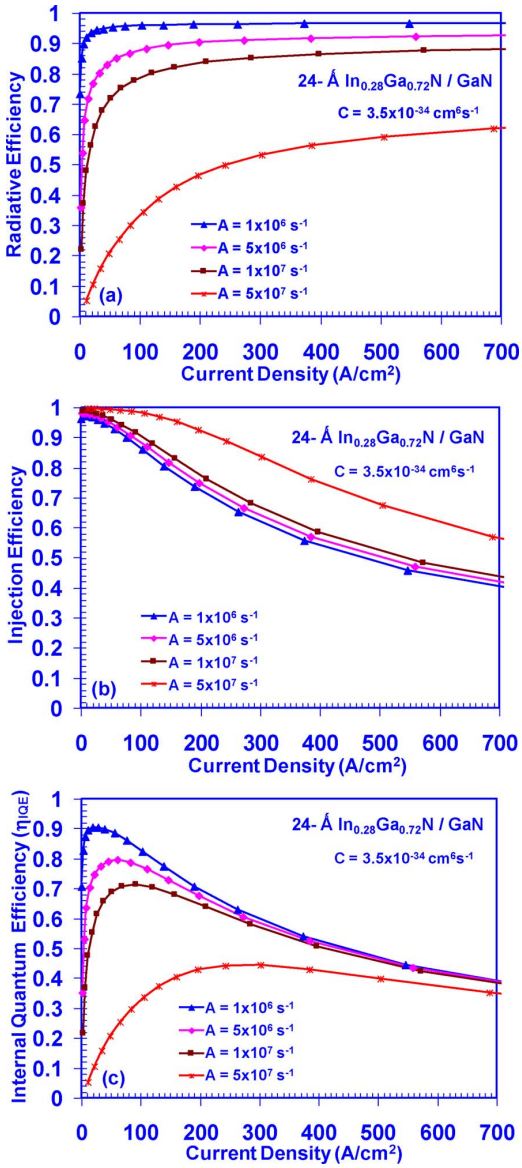

Fig. 5. (a) Radiative efficiency ($\eta_{Radiative}$), (b) current injection efficiency ($\eta_{Injection}$) and c) IQE of 24-Å $In_{0.28}Ga_{0.72}N$-GaN QW plotted at various monomolecular recombination coefficients ($A = 1 \times 10^6$ s^{-1}, 5×10^6 s^{-1}, 1×10^7 s^{-1} and 5×10^7 s^{-1}). Auger recombination coefficient keeps as constant $C = 3.5 \times 10^{-34}$ cm^6/s.

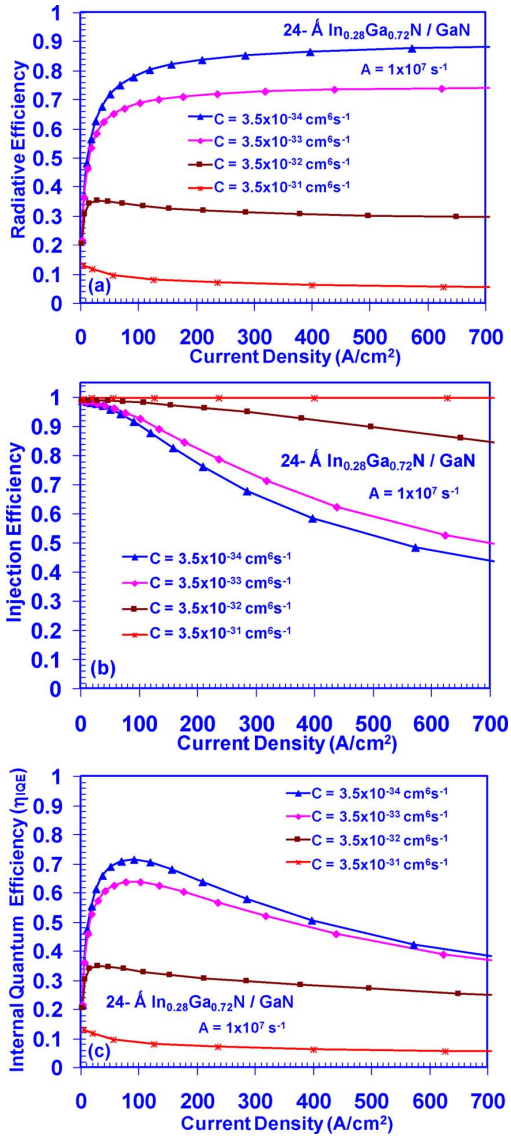

Fig. 6. (a) Radiative efficiency ($\eta_{Radiative}$), (b) current injection efficiency ($\eta_{Injection}$) and c) IQE of 24-Å $In_{0.28}Ga_{0.72}N$-GaN QW plotted at various Auger recombination coefficients ($C = 3.5 \times 10^{-34}$ cm^6/s, 3.5×10^{-33} cm^6/s, 3.5×10^{-32} cm^6/s and 3.5×10^{-31} cm^6/s). Monomolecular recombination coefficient keeps as constant $A = 1 \times 10^7$ s^{-1}.

$A = 1 \times 10^6$ s^{-1} were used for the calculations in Figs. 6 and 7, respectively. The internal quantum efficiency (η_{IQE}) is the product of the radiative efficiency ($\eta_{Radiative}$) and current injection efficiency ($\eta_{Injection}$), which were plotted versus the total current density (J_{tot}) in Figs. 6(c) and 7(c), respectively.

From Figs. 6(b) and 7(b), the current injection efficiency ($\eta_{Injection}$) increases as the Auger recombination coefficient (C) increases due to the reduction of the nonradiative carrier lifetime, which is similar to the effect of the monomolecular recombination coefficient (A) on the current injection efficiency ($\eta_{Injection}$) as shown in Fig. 5(b). However, the effect of the Auger recombination coefficient (C) on the radiative efficiency ($\eta_{Radiative}$) is more influential than that of the monomolecular recombination coefficient (A) due to the fact that the Auger recombination term is proportional to the cube of the carrier density ($R_{Auger} = C \cdot N^3$). Note that the large Auger recombination coefficient (C) suppresses the radiative efficiency ($\eta_{Radiative}$), which results in the reduction of the internal quantum efficiency (η_{IQE}) as shown in Figs. 6(c) and 7(c).

D. Effect of GaN Hole Mobility (μ_p) on Efficiency Droop

The impact of the GaN hole mobility (μ_p) on the current injection efficiency ($\eta_{Injection}$) and internal quantum efficiency (η_{IQE}) is investigated. The calculation results based on three different GaN hole mobility (μ_p) of 22 $cm^2/(V \cdot s)$, 50 $cm^2/(V \cdot s)$ and 300 $cm^2/(V \cdot s)$ are plotted in Fig. 8. Note that in this calculation the monomolecular recombination coefficient $A = 1 \times 10^6$ s^{-1} and Auger recombination coefficient $C = 3.5 \times 10^{-34}$ cm^6/s were used.

From Fig. 8, the current injection efficiency ($\eta_{Injection}$) is enhanced as the GaN hole mobility (μ_p) increases. However, the

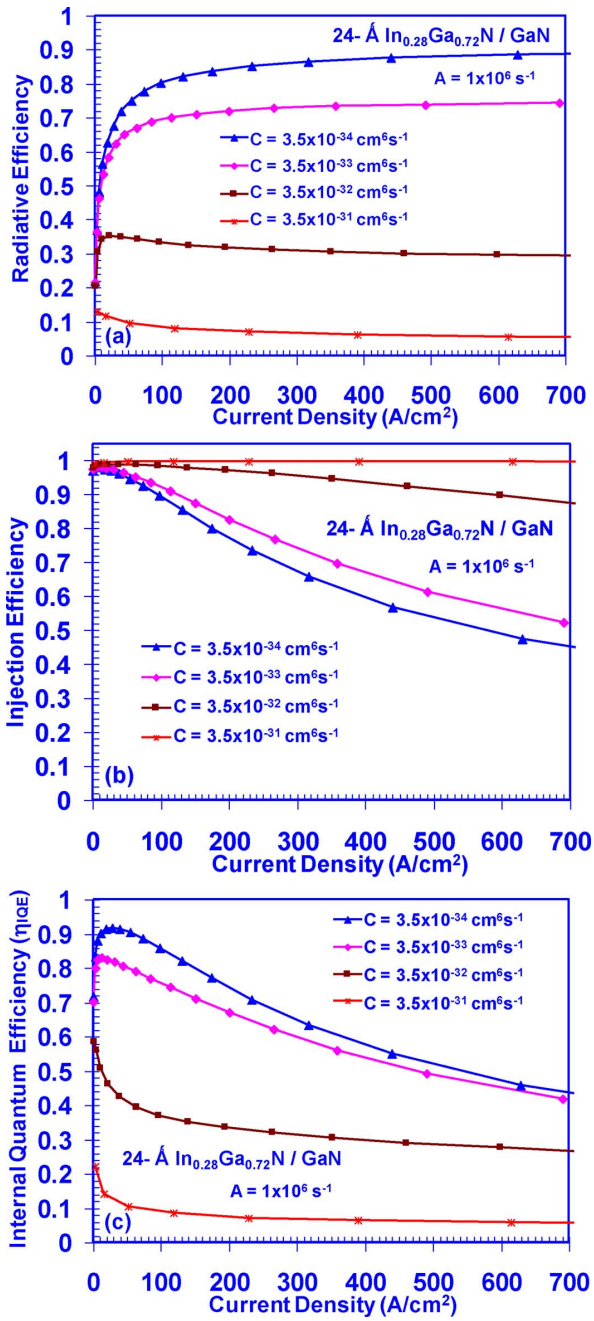

Fig. 7. (a) Radiative efficiency ($\eta_{Radiative}$), (b) current injection efficiency ($\eta_{Injection}$) and c) IQE of 24-Å $In_{0.28}Ga_{0.72}N$-GaN QW plotted at various Auger recombination coefficients ($C = 3.5 \times 10^{-34}$ cm^6/s, 3.5×10^{-33} cm^6/s, 3.5×10^{-32} cm^6/s and 3.5×10^{-31} cm^6/s). Monomolecular recombination coefficient keeps as constant $A = 1 \times 10^6$ s^{-1}.

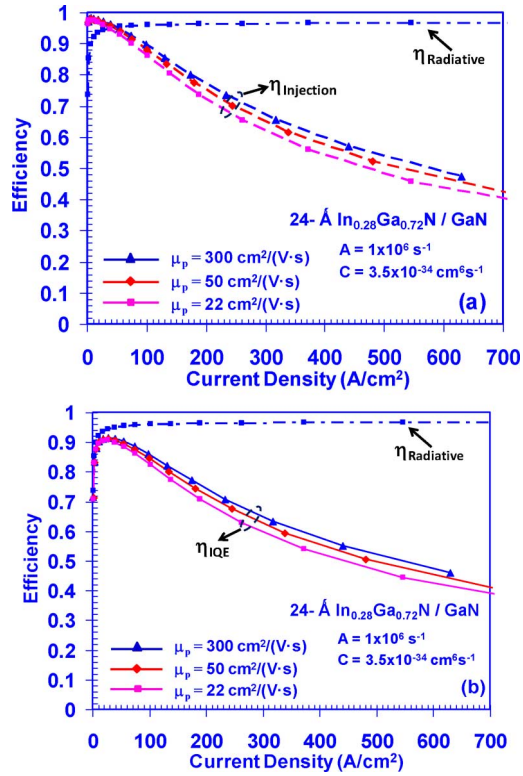

Fig. 8. (a) Radiative efficiency ($\eta_{Radiative}$) and current injection efficiency ($\eta_{Injection}$) and (b) radiative efficiency ($\eta_{Radiative}$) and IQE of 24-Å $In_{0.28}Ga_{0.72}N$-GaN QW plotted at various GaN hole mobilities ($\mu_p = 22$ cm$^2/(\mathrm{V} \cdot \mathrm{s})$, 50 cm$^2/(\mathrm{V} \cdot \mathrm{s})$ and 300 cm$^2/(\mathrm{V} \cdot \mathrm{s})$).

increase of the GaN hole mobility did not reduce the efficiency droop. The impact of the GaN hole mobility on the current injection efficiency ($\eta_{Injection}$) is relatively minimal. From the experiment aspect, the GaN hole mobility depends on the material quality, and typically the GaN hole mobility (μ_p) is 1–2 order of magnitude lower than that for electron (μ_n). Thus, based on our finding, the efficiency droop in InGaN-GaN QW LEDs is not attributed to the lower GaN hole mobility. Higher hole mobility will improve the carrier transport in the InGaN – GaN QW LEDs, however the enhancement in the current injection efficiency and internal quantum efficiency will be minimal at high operating current density.

V. Approaches to Suppress Efficiency Droop in Nitride LEDs

A. Use of Thin Large Bandgap Barriers in InGaN QW LEDs

From the previous discussion, the issues of efficiency droop of InGaN QW LEDs appear to result from the quenching of current injection efficiency ($\eta_{Injection}$) attributed to the increase in thermionic carrier escape rate at high injection current. Thus, to suppress the efficiency-droop observed in InGaN QW LEDs, novel QW-barrier designs with significant suppression of thermionic carrier escape at high current density are required. In the proposed structures, we employed thin (15-Å) larger energy bandgap materials such as $Al_xGa_{1-x}N$, $Al_xIn_{1-x}N$ or $Al_xIn_yGa_{1-x-y}N$ surrounding the InGaN QW active region as shown in Fig. 9. The use of thin larger energy bandgap barriers sandwiched between GaN barriers and InGaN QW active region leads to significant suppression of the efficiency-droop in III-Nitride LEDs.

B. InGaN QW LEDs With $Al_{0.1}Ga_{0.9}N$ or $Al_{0.83}In_{0.17}N$ Thin Barriers

Fig. 10 shows the comparison of the injection efficiency ($\eta_{Injection}$) as a function of the total current density for 24-Å $In_{0.28}Ga_{0.72}N$ QW employing the 15-Å $Al_{0.1}Ga_{0.9}N$ barriers or 15-Å $Al_{0.83}In_{0.17}N$ barriers surrounding the QW. Low Al-content (10%) AlGaN material is slightly tensile strain

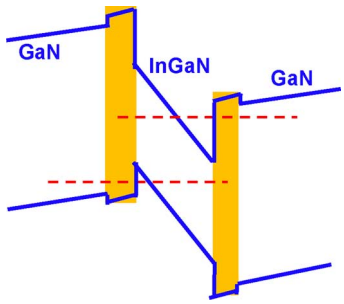

Fig. 9. Schematic of the InGaN-GaN QW structure inserted with large bandgap barriers.

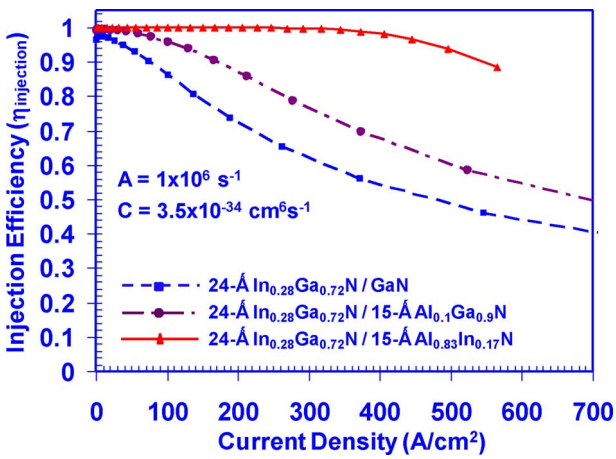

Fig. 10. Injection efficiency ($\eta_{Injection}$) as a function of total current density for 24-Å $In_{0.28}Ga_{0.72}N$/ GaN QW, 24-Å $In_{0.28}Ga_{0.72}N$/15-Å $Al_{0.1}Ga_{0.9}N$ QW and 24-Å $In_{0.28}Ga_{0.72}N$/15-Å $Al_{0.83}In_{0.17}N$ QW.

with respect to GaN. The $Al_{0.83}In_{0.17}N$ material is employed in the second design due to the lattice-matching condition of this alloy to GaN. Note that the entire InGaN/AlGaN QW and InGaN/AlInN QW systems are surrounded by u-GaN layer. Both the thicknesses of the upper and lower barrier layers for all the structures investigated here are 10 nm. The comparison indicates that the quenching of the current injection efficiency for the InGaN/AlGaN QW LED is reduced at high carrier density or high current density, in comparison to that of InGaN-GaN QW LED. The InGaN/AlInN QW LED structure shows almost no droop up to carrier density of 13×10^{19} cm^{-3} or current density of $J_{tot} \sim 450$ A/cm^2 due to the use of thin lattice-matched $Al_{0.83}In_{0.17}N$ ($E_g \sim 4.51$ eV) barriers.

Fig. 11 shows the radiative efficiency ($\eta_{Radiative}$), current injection efficiency ($\eta_{Injection}$), and the internal quantum efficiency (η_{IQE}) as a function of the total current density (J_{tot}) for 24-Å $In_{0.28}Ga_{0.72}N$/15-Å $Al_{0.1}Ga_{0.9}N$ QW, respectively. The inset of Fig. 11 shows the energy band lineup for the InGaN/AlGaN QW structure, surrounded by u-GaN barrier layers. By utilizing the InGaN/AlGaN QW structure, the radiative efficiency ($\eta_{Radiative}$) is enhanced due to the enhanced spontaneous emission radiative recombination rate as compared to that of the conventional InGaN – GaN QW [16]. In addition to this, the current injection efficiency ($\eta_{Injection}$) of the InGaN/AlGaN is improved as well due to stronger thermionic carrier suppression from the use of the thin layer of higher AlGaN

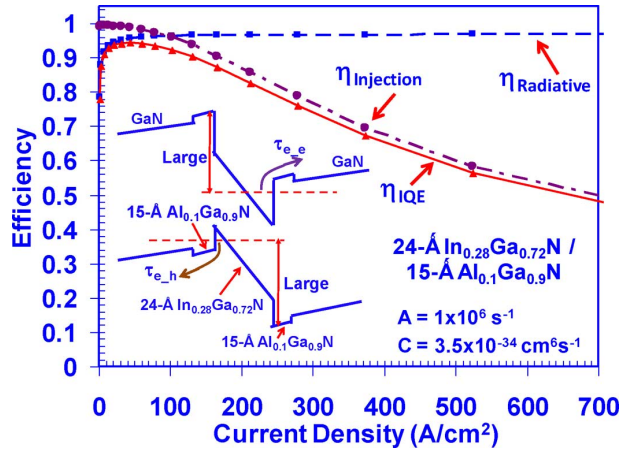

Fig. 11. IQE (η_{IQE}) of 24-Å $In_{0.28}Ga_{0.72}N$/15-Å $Al_{0.1}Ga_{0.9}N$ QW ($\lambda \sim$ 480 nm) at 300 K. IQE (η_{IQE}), radiative efficiency ($\eta_{Radiative}$) and current injection efficiency ($\eta_{Injection}$) as a function of total current density are plotted.

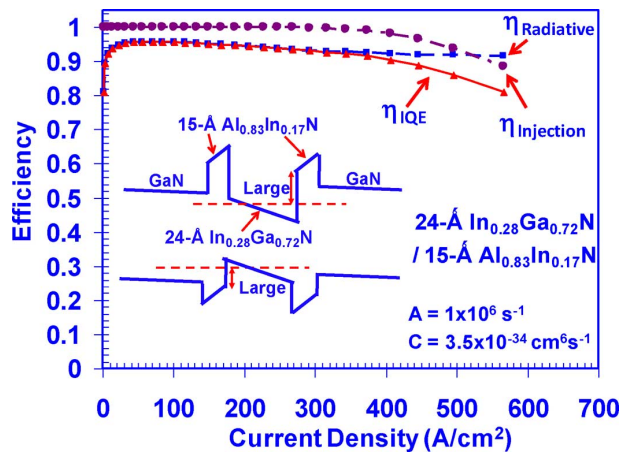

Fig. 12. IQE (η_{IQE}) of 24-Å $In_{0.28}Ga_{0.72}N$/15-Å $Al_{0.83}In_{0.17}N$ QW ($\lambda \sim$ 480 nm) at 300 K. IQE (η_{IQE}), radiative efficiency ($\eta_{Radiative}$) and current injection efficiency ($\eta_{Injection}$) as a function of carrier density are plotted.

barrier as compared to that of the conventional InGaN – GaN QW structure. Thus, the internal quantum efficiency (η_{IQE}) for InGaN/AlGaN LEDs reaches its peak at $J_{peak} \sim 30 \sim 50$ A/cm^2, and the IQE reduces by 34% from its peak efficiency at $J_{tot} \sim 450$ A/cm^2. The use of thin AlGaN barrier layers enables the InGaN QW LEDs to operate with higher J_{peak} and slight reduction in efficiency droop.

Fig. 12 shows the radiative efficiency ($\eta_{Radiative}$), current injection efficiency ($\eta_{Injection}$), and the internal quantum efficiency (η_{IQE}) as a function of the total current density (J_{tot}) for 24-Å $In_{0.28}Ga_{0.72}N$/15-Å $Al_{0.83}In_{0.17}N$ QW. The inset of Fig. 12 shows the energy band lineups for the InGaN/AlInN QW structure, which is surrounded by u-GaN barrier layers. By utilizing the larger band gap material of AlInN as the thin barriers to surround the InGaN QW, the injection efficiency ($\eta_{Injection}$) is significantly enhanced. The use of InGaN/AlInN QW LEDs leads to high injection efficiency with very minimum droop up to current density above 450 A/cm^2. Thus, the internal quantum efficiency (η_{IQE}) of the InGaN/AlInN QW LED device starts to drop at $J_{peak} \sim 400$ A/cm^2. The internal quantum efficiency (η_{IQE}) is reduced by only 15% from its peak efficiency value

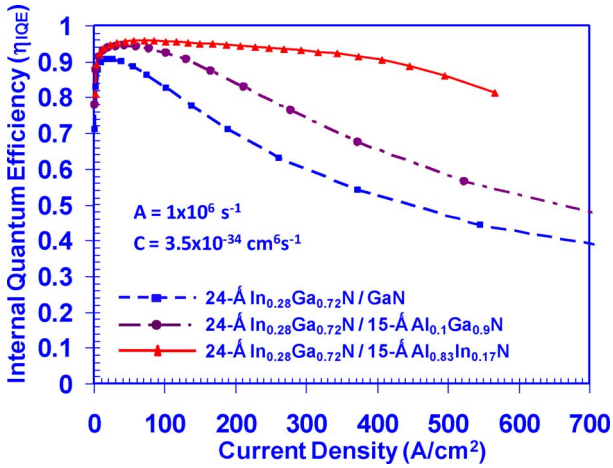

Fig. 13. IQE (η_{IQE}) as a function of total current density for 24-Å $In_{0.28}Ga_{0.72}N$/ GaN QW, 24-Å $In_{0.28}Ga_{0.72}N$/15-Å $Al_{0.1}Ga_{0.9}N$ QW and 24-Å $In_{0.28}Ga_{0.72}N$/15-Å $Al_{0.83}In_{0.17}N$ QW.

at $J_{tot} \sim 580$ A/cm^2. Note that the radiative efficiency of the InGaN/AlInN QW structure is slightly lower as compared to that of the conventional InGaN – GaN QW due to the existence of only one confined state in the QW. However, due to the much superior injection efficiency from InGaN/AlInN QW LEDs, the IQE is enhanced significantly at high operating current density.

Fig. 13 shows the comparison of the internal quantum efficiency (η_{IQE}) for three QW structures (24-Å $In_{0.28}Ga_{0.72}N$/GaN QW, 24-Å $In_{0.28}Ga_{0.72}N$/15-Å $Al_{0.1}Ga_{0.9}N$ QW and 24-Å $In_{0.28}Ga_{0.72}N$/15-Å $Al_{0.83}In_{0.17}N$ QW), which show the enhancement of the IQE for the QW structures with thin barrier layers of $Al_{0.1}Ga_{0.9}N$ or $Al_{0.83}In_{0.17}N$ barriers. Slight enhancement of the IQE is observed for the InGaN QW LED structure employing thin AlGaN barriers. The use of AlInN barrier layers leads to higher IQE and minimum efficiency droop throughout a large current density range up to high current density of J > 450 A/cm^2.

C. Effects of $Al_{0.1}Ga_{0.9}N$ or $Al_{0.83}In_{0.17}N$ Barrier Thickness on IQE of InGaN QW LEDs

In this section, the effects of the $Al_{0.1}Ga_{0.9}N$ or $Al_{0.83}In_{0.17}N$ barriers on current injection efficiency ($\eta_{Injection}$) and internal quantum efficiency (η_{IQE}) are investigated. Fig. 14(a) shows the injection efficiencies ($\eta_{Injection}$) of 24-Å $In_{0.28}Ga_{0.72}N$ QW surrounded by d-Å $Al_{0.83}In_{0.17}N$ barriers with d = 5 Å, 10 Å, 15 Å, 20 Å and 25 Å. The results are compared with the conventional 24-Å $In_{0.28}Ga_{0.72}N$ QW with GaN barriers. As shown in Fig. 14(a), the injection efficiency ($\eta_{Injection}$) increases as the thickness of $Al_{0.1}Ga_{0.9}N$ barrier increases due to the suppression of the thermionic carrier leakage from the QW to the barrier regions. Fig. 14(b) plots the corresponding internal quantum efficiency (η_{IQE}) as a function of the total current density, which shows the similar trend as Fig. 14(a).

Note that it is challenging to employ AlGaN as barrier materials surrounding the InGaN QWs due to the large discrepancy of the optimized growth temperature between InGaN QW ($T_g \sim 740$ °C) and AlGaN barriers ($T_g \sim 1080$°C) [57], [58].

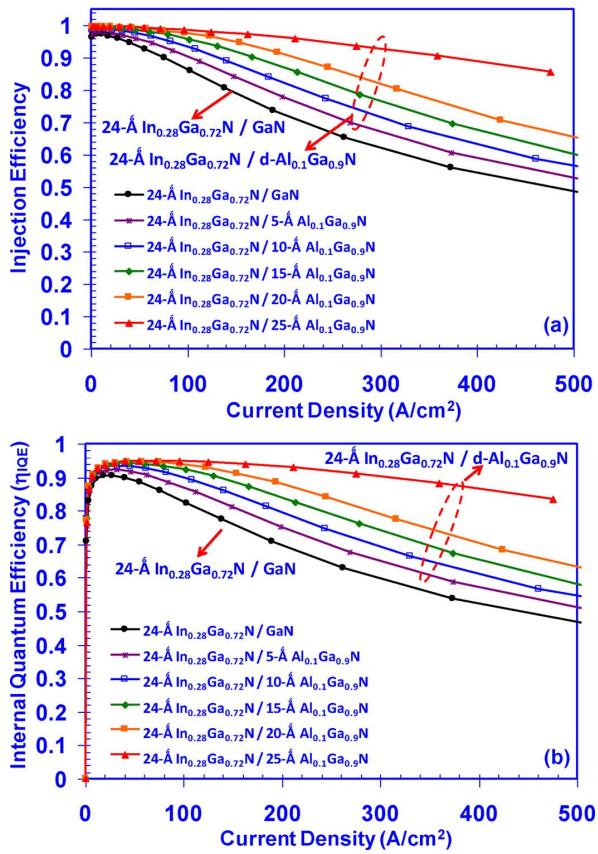

Fig. 14. (a) Injection efficiency ($\eta_{Injection}$) and (b) IQE as a function of total current density for 24-Å $In_{0.28}Ga_{0.72}N$/GaN QW, 24-Å $In_{0.28}Ga_{0.72}N$/d -Å $Al_{0.1}Ga_{0.9}N$ QW with d = 5 Å, 10 Å, 15 Å, 20 Å, and 25 Å.

Thus, the use of low Al-content (10%) and very thin layers of AlGaN barriers are important for enabling the growth of high-quality InGaN/AlGaN QW structure.

Fig. 15(a) and (b) show the injection efficiency ($\eta_{Injection}$) [Fig. 15(a)] and internal quantum efficiency (η_{IQE}) [Fig. 15(b)] versus the total current density (J_{tot}) of 24-Å $In_{0.28}Ga_{0.72}N$ QW surrounded by d $Al_{0.83}In_{0.17}N$ barriers with d = 5-Å, 10-Å, 15-Å, 20-Å and 25-Å. The results are compared to that of the conventional 24-Å $In_{0.28}Ga_{0.72}N$ QW with GaN barriers. Fig. 15(a) indicates that the current injection efficiency ($\eta_{Injection}$) is significantly enhanced when the thickness of the $Al_{0.83}Ga_{0.17}N$ barrier is larger than 10-Å. The current injection efficiency ($\eta_{Injection}$) reaches its maximum when the thickness of the $Al_{0.83}In_{0.17}N$ barrier is thicker than 15-Å, and there is almost no reduction of the injection efficiency ($\eta_{Injection}$).

Fig. 15(b) shows the comparison of the internal quantum efficiency (η_{IQE}) for 24-Å $In_{0.28}Ga_{0.72}N$/d-Å $Al_{0.83}In_{0.17}N$ QW. The figure shows that the internal quantum efficiency (η_{IQE}) exhibits less droop as the AlInN barrier is thicker. When d > 15-Å, the internal quantum efficiency (η_{IQE}) shows no droop as the current density increases. One more important advantage to utilize InGaN/AlInN structure as compared to InGaN/AlGaN structure is that AlInN ternary is able to be grown at similar temperature, which ranges from $T_g \sim 750$°C up to $T_g \sim 780$°C [59]–[61] as InGaN QW. Thus, the efficiency droop issue in nitride LEDs has potential to be resolved by employing thin layers

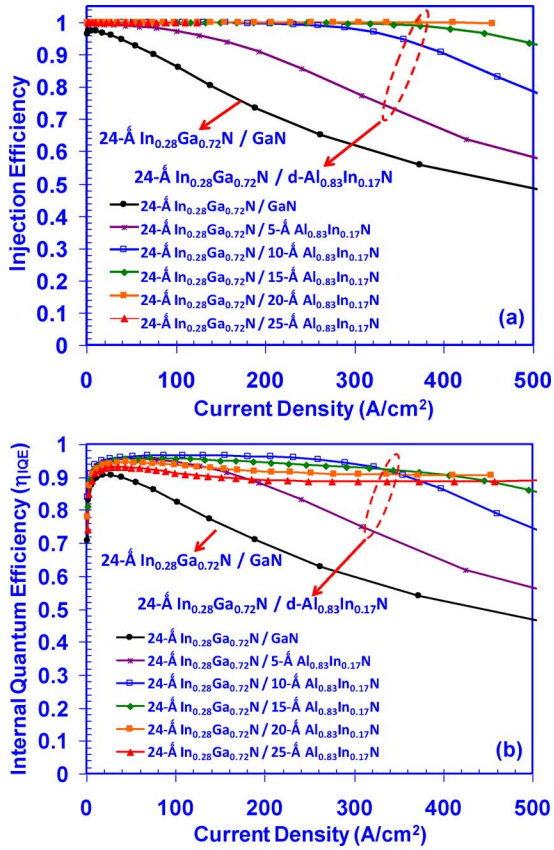

Fig. 15. (a) Injection efficiency ($\eta_{Injection}$) and (b) IQE as a function of total current density for 24-Å $In_{0.28}Ga_{0.72}N$/GaN QW, 24-Å $In_{0.28}Ga_{0.72}N$/d $Al_{0.83}In_{0.17}N$ QW with d = 5 Å, 10-Å, 15-Å, 20-Å, and 25-Å.

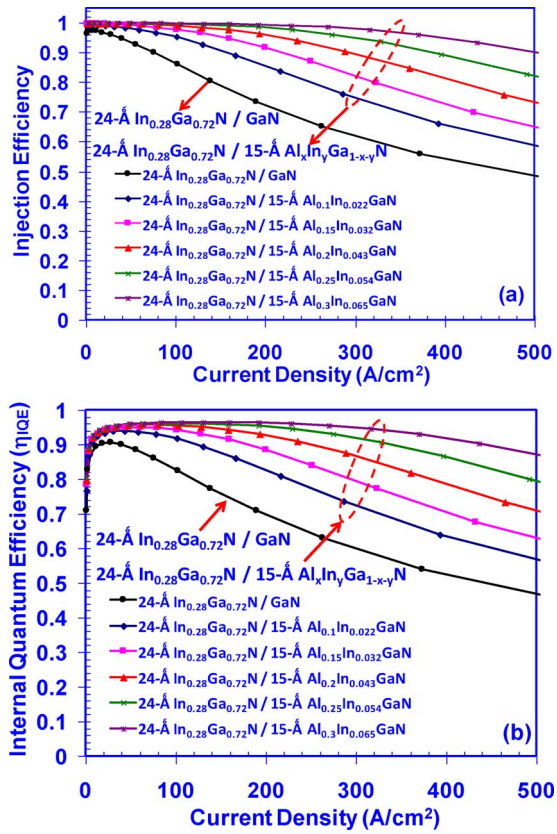

Fig. 16. (a) Injection efficiency ($\eta_{Injection}$) and (b) IQE as a function of total current density for 24-Å $In_{0.28}Ga_{0.72}N$/GaN QW, 24-Å $In_{0.28}Ga_{0.72}N$/15-Å $In_xIn_yGa_{1-x-y}N$ ($x = 4.66y$) QW with $x = 0.1$, 0.15, 0.2, 0.25, 0.3.

of AlInN barriers sandwiched between the InGaN QW and GaN barriers.

D. Characteristics of InGaN QW LEDs With Lattice-Matched $Al_xIn_yGa_{1-x-y}N$ Thin Barriers

The lattice-matching condition for $A_xIn_yGa_{1-x-y}N$ to GaN requires $x = 4.66y$, and Table I lists five different Al-contents (and In-contents) $Al_xIn_yGa_{1-x-y}N$ and their corresponding energy bandgaps that satisfy the lattice-matching condition. Fig. 16(a) and (b) show the comparison of the injection efficiency ($\eta_{Injection}$) [Fig. 16(a)] and internal quantum efficiency [Fig. 16(b)] versus the total current density (J_{tot}) for 24-Å $In_{0.28}Ga_{0.72}N$/15-Å $Al_xIn_yGa_{1-x-y}N$ QW with $x = 0.1$, 0.15, 0.2, 0.25, and 0.3. The results are compared with the conventional 24-Å $In_{0.28}Ga_{0.72}N$/GaN QW. As the Al-content increases, the energy bandgap for lattice-matched quaternary AlInGaN increases, which leads to stronger suppression of the thermionic carrier leakage. Thus, the quenching of injection efficiency ($\eta_{Injection}$) for 24-Å $In_{0.28}Ga_{0.72}N$/15-Å $Al_xIn_yGa_{1-x-y}N$ QW decreases as Al-content (x) increases as shown in Fig. 16(a). Fig. 16(b) shows the comparison of the internal quantum efficiency (η_{IQE}) as a function of the total current density (J_{tot}) for 24-Å $In_{0.28}Ga_{0.72}N$/15-Å $Al_xIn_yGa_{1-x-y}N$ QW with $x = 0.1$, 0.15, 0.2, 0.25, and 0.3. The radiative efficiencies ($\eta_{Radiative}$) for 24-Å $In_{0.28}Ga_{0.72}N$/15-Å $Al_xIn_yGa_{1-x-y}N$ QW with different Al-content are similar. Therefore, the internal quantum efficiency (η_{IQE}) [Fig. 16(b)] shows the similar trend as the injection efficiency ($\eta_{Injection}$) [Fig. 16(a)].

Recently, InGaN QWs employing polarization matched quaternary AlInGaN thick barriers instead of GaN barriers have been suggested as a method to suppress the droop issue [18], [62]. The corresponding experimental works had been reported for MOCVD-grown InGaN QW LEDs with thick ($\sim$ 10 nm) quaternary AlInGaN barrier materials [18], [37], [63] as polarization matched barriers, which resulted in suppression of efficiency droop.

In our approach, much thinner layers ($\sim$ 1 nm – 2 nm) large-bandgap AlInGaN or AlInN materials are shown as sufficient for suppressing the thermionic carrier escape process, which in turn results in reduced efficiency droop phenomenon. The growths of thin AlInN or AlInGaN barrier materials will be more compatible in LED manufacturing process. The lattice-matching condition enables the reduction of the misfit dislocations. In addition, the growths of AlInGaN material were performed at similar temperature as that of InGaN QW. In addition, recent works have also shown the suppression of polarization field by growing the GaN-based LEDs on semi-polar orientation [64], [65] had resulted in improved effective barrier height, which in turn results in reduced efficiency droop up to J $\sim$ 200 A/cm^2.

The investigation of injection efficiency in this work was based on the analytical equations articulated from the current continuity relations. The use of this analytical relation [20], [40]

discussed here provides physically-intuitive results applicable in understanding the droop phenomena and injection efficiency in nitride LEDs. Note that the direct measurement to separate the contributions of current injection and radiative efficiencies in QW LEDs/lasers is challenging. However, the measurements of the thermionic carrier escape rate in QW lasers/LEDs, which is strongly correlated to the current injection quenching, had recently been performed by using two-color pump probe experiments [66]. In addition, the carrier transport and recombination processes can be taken into account by using numerical simulation. The approach of using thin large-bandgap material for efficiency droop suppression is also investigated by APSYS simulation with the consideration of carrier transport effect in the device configurations [39]. The simulation results are in good agreement with our conclusion that the insertion of lattice-matched AlInGaN thin barriers ($\sim$ 1.5-nm) would greatly suppress the carrier leakage and enhance the IQE of InGaN QW LEDs at high current density.

VI. Summary

In summary, we have analyzed current injection efficiency and internal quantum efficiency in InGaN QW LEDs. The use of analytical relation [40] for describing the current injection efficiency in nitride-based QWs LEDs results in more physically-intuitive method applicable for understanding the droop phenomenon in the devices. The injection efficiency is found to reach its peak at low current density and decreases gradually with increasing current, thus consistent with the problem of efficiency droop in III-Nitride LEDs. Increasing monomolecular recombination coefficient and Auger recombination coefficient lead to the reduction of radiative efficiency and increase of the injection efficiency, which results in the reduction of the quenching of the efficiency droop with lower peak internal quantum efficiency.

The utilization of thin low Al-content AlGaN layer as the QW barrier leads to slight reduction in quenching of the injection efficiency as compared to that of the conventional InGaN QW. By employing the thin-layer of lattice-matched $Al_{0.83}In_{0.17}N$ or lattice-matched $Al_xIn_yGa_{1-x-y}N$ barriers, the injection efficiency shows relatively minimum droop up to very high current density ($J_{tot} > 450$ A/cm^2), which provides possible solution for the efficiency droop issue in high-power nitride LEDs.

References

[1] S. F. Chichibu, T. Azuhata, M. Sugiyama, T. Kitamura, Y. Ishida, H. Okumura, H. Nakanishi, T. Sota, and T. Mukai, "Optical and structural studies in InGaN quantum well structure laser diodes," *J. Vacuum Sci. & Technol. B*, vol. 19, pp. 2177–2183, Nov.-Dec. 2001.

[2] S. Nakamura, M. Senoh, S. Nagahama, N. Iwasa, T. Yamada, T. Matsushita, H. Kiyoku, and Y. Sugimoto, "InGaN-based multi-quantum-well-structure laser diodes," *Jpn. J. Appl. Phys.*, vol. 35, pt. 2, pp. L74–L76, Jan. 1996.

[3] J. Zhang *et al.*, "Enhanced luminescence in InGaN multiple quantum wells with quaternary AlInGaN barriers," *Appl. Phys. Lett.*, vol. 77, pp. 2668–2670, 2000.

[4] X. Guo, Y.-L. Li, and E. F. Schubert, "Efficiency of GaN/InGaN light-emitting diodes with interdigitated mesa geometry," *Appl. Phys. Lett.*, vol. 79, pp. 1936–1938, 2001.

[5] S. H. Park, D. Ahn, and S. L. Chuang, "Electronic and optical properties of a- and m-plane wurtzite InGaN– GaN quantum wells," *IEEE J. Quantum Electron.*, vol. 43, pp. 1175–1182, 2007.

[6] R. M. Farrell, E. C. Young, F. Wu, S. P. DenBaars, and J. S. Speck, "Materials and growth issues for high-performance nonpolar and semipolar light-emitting devices," *Semicond. Sci. Technol.*, vol. 27, no. 2, Feb. 2012, Art. 024001.

[7] R. A. Arif, Y. K. Ee, and N. Tansu, "Polarization engineering via staggered InGaN quantum wells for radiative efficiency enhancement of light emitting diodes," *Appl. Phys. Lett.*, vol. 91, p. 091110, Aug. 2007.

[8] H. Zhao, G. Y. Liu, J. Zhang, J. D. Poplawsky, V. Dierolf, and N. Tansu, "Approaches for high internal quantum efficiency green InGaN light-emitting diodes with large overlap quantum wells," *Opt. Express*, vol. 19, no. S4, pp. A991–A1007, Jul. 2011.

[9] H. Zhao, G. Y. Liu, X. H. Li, R. A. Arif, G. S. Huang, J. D. Poplawsky, S. T. Penn, V. Dierolf, and N. Tansu, "Design and characteristics of staggered InGaN quantum-well light-emitting diodes in the green spectral regime," *IET Optoelectron.*, vol. 3, pp. 283–295, Dec. 2009.

[10] S.-H. Park, D. Ahn, B.-H. Koo, and J.-W. Kim, "Dip-shaped InGaN/GaN quantum-well light-emitting diodes with high efficiency," *Appl. Phys. Lett.*, vol. 95, p. 063507, 2009.

[11] C. T. Liao, M. C. Tsai, B. T. Liou, and Y. K. Kuo, "Improvement in output power of a 460 nm InGaN light-emitting diode using staggered quantum well," *J. Appl. Phys.*, vol. 108, no. 6, Art. 063107, Sep. 2010.

[12] L. Y. Zhang, K. Cheng, H. Liang, R. Lieten, M. Leys, and G. Borghs, "Photoluminescence studies of polarization effects in InGaN/(In)GaN multiple quantum well structures," *Jpn. J. Appl. Phys.*, vol. 51, no. 3, Art. 030207, Mar. 2012.

[13] R. A. Arif, H. Zhao, and N. Tansu, "Type-II InGaN-GaNAs quantum wells for lasers applications," *Appl. Phys. Lett.*, vol. 92, p. 011104, 2008.

[14] H. Zhao, R. A. Arif, and N. Tansu, "Self-consistent gain analysis of type-II 'W' InGaN–GaNAs quantum well lasers," *J. Appl. Phys.*, vol. 104, p. 043104, 2008.

[15] S. H. Park, Y. T. Lee, and J. Park, "Optical properties of type-II InGaN/GaAsN/GaN quantum wells," *Opt. Quantum Electron.*, vol. 41, no. 11–13, pp. 779–785, Nov. 2009.

[16] H. Zhao, G. Liu, and N. Tansu, "Analysis of InGaN-delta-InN quantum wells for light-emitting diodes," *Appl. Phys. Lett.*, vol. 97, p. 131114, 2010.

[17] M. F. Schubert, S. Chhajed, J. K. Kim, E. F. Schubert, D. D. Koleske, M. H. Crawford, S. R. Lee, A. J. Fischer, G. Thaler, and M. A. Banas, "Effect of dislocation density on efficiency droop in GaInN/GaN light-emitting diodes," *Appl. Phys. Lett.*, vol. 91, p. 231114, 2007.

[18] M. F. Schubert *et al.*, "Polarization matched GaInN/AlGaInN multi-quantum-well light emitting diodes with reduced efficiency droop," *Appl. Phys. Lett.*, vol. 93, p. 041102, 2008.

[19] J. Xu *et al.*, "Reduction in efficiency droop, forward voltage, ideality factor, and wavelength shift in polarization matched GaInN/GaInN multi quantum well light-emitting diodes," *Appl. Phys. Lett.*, vol. 94, p. 011113, 2009.

[20] H. Zhao, G. Y. Liu, R. A. Arif, and N. Tansu, "Current injection efficiency induced efficiency-droop in InGaN quantum well light-emitting diodes," *Solid-State Electron.*, vol. 54, pp. 1119–1124, Oct. 2010.

[21] G.-B. Lin, D. Meyaard, J. Cho, E. F. Schubert, H. Shim, and C. Sone, "Analytic model for the efficiency droop in semiconductors with asymmetric carrier-transport properties based on drift-induced reduction of injection efficiency," *Appl. Phys. Lett.*, vol. 100, p. 161106, 2012.

[22] J. Wang, L. Wang, L. Wang, Z. Hao, Y. Luo, A. Dempewolf, M. Muller, F. Bertram, and J. Christen, "An improved carrier rate model to evaluate internal quantum efficiency and analyze efficiency droop origin of InGaN based light-emitting diodes," *J. Appl. Phys.*, vol. 112, p. 023107, 2012.

[23] I. E. Titkov *et al.*, "Blue light emitting diode internal and injection efficiency," *AIP Adv.*, vol. 2, p. 032117, 2012.

[24] J. Xie, X. Ni, Q. Fan, R. Shimada, U. Ozgur, and H. Morkoc, "On the efficiency droop in InGaN multiple quantum well blue light emitting diodes and its reduction with p-doped quantum well barriers," *Appl. Phys. Lett.*, vol. 93, p. 121107, 2008.

[25] X. F. Ni, Q. Fan, R. Shimada, U. Ozgur, and H. Morkoc, "Reduction of efficiency droop in InGaN light emitting diodes by coupled quantum wells," *Appl. Phys. Lett.*, vol. 93, p. 171113, 2008.

[26] M. Maier, K. Kohler, M. Kunzer, W. Pletschen, and J. Wagner, "Reduced nonthermal rollover of wide-well GaInN light-emitting diodes," *Appl. Phys. Lett.*, vol. 94, p. 041103, 2009.

[27] Y. C. Shen, G. O. Mueller, S. Watanabe, N. F. Gardner, A. Munkholm, and M. R. Krames, "Auger recombination in InGaN measured by photoluminescence," *Appl. Phys. Lett.*, vol. 91, p. 141101, Oct. 2007.

[28] N. F. Gardner, G. O. Muller, Y. C. Shen, G. Chen, S. Watanabe, W. Gotz, and M. R. Krames, "Blue-emitting InGaN–GaN double-heterostructure light-emitting diodes reaching maximum quantum efficiency above 200 A/cm^2," *Appl. Phys. Lett.*, vol. 91, p. 243506, 2007.
[29] K. T. Delaney, P. Rinke, and C. G. V. d. Walle, "Auger recombination rates in nitrides from first principles," *Appl. Phys. Lett.*, vol. 94, p. 191109, 2009.
[30] E. Kioupakis, P. Rinke, A. Schleife, F. Bechstedt, and C. G. Van de Walle, "Free-carrier absorption in nitrides from first principles," *Phys. Rev. B*, vol. 81, Jun. 2010.
[31] E. Kioupakis, P. Rinke, K. T. Delaney, and C. G. Van de Walle, "Indirect Auger recombination as a cause of efficiency droop in nitride light-emitting diodes," *Appl. Phys. Lett.*, vol. 98, p. 161107, Apr. 2011.
[32] A. Efremov, N. Bochkareva, R. Gorbunov, D. Lavrinovich, Y. Rebane, D. Tarkhin, and Y. Shreter, "Effect of the joule heating on the quantum efficiency and choice of thermal conditions for high-power blue InGaN/GaN LEDs," *Semiconductors*, vol. 40, pp. 605–610, 2006.
[33] J. Y. Chang and Y. K. Kuo, "Influence of polarization-matched AlGaInN barriers in blue InGaN light-emitting diodes," *Optics Lett.*, vol. 37, pp. 1574–1576, May 2012.
[34] S. Choi, H. J. Kim, S. S. Kim, J. Liu, J. Kim, J. H. Ryou, R. D. Dupuis, A. M. Fischer, and F. A. Ponce, "Improvement of peak quantum efficiency and efficiency droop in III-nitride visible light-emitting diodes with an InAlN electron-blocking layer," *Appl. Phys. Lett.*, vol. 96, p. 221105, 2010.
[35] Y. K. Kuo, J. Y. Chang, and M. C. Tsai, "Enhancement in hole-injection efficiency of blue InGaN light-emitting diodes from reduced polarization by some specific designs for the electron blocking layer," *Opt. Lett.*, vol. 35, pp. 3285–3287, Oct. 2010.
[36] C. H. Wang, S. P. Chang, W. T. Chang, J. C. Li, Y. S. Lu, Z. Y. Li, H. C. Yang, H. C. Kuo, T. C. Lu, and S. C. Wang, "Efficiency droop alleviation in InGaN/GaN light-emitting diodes by graded-thickness multiple quantum wells," *Appl. Phys. Lett.*, vol. 97, p. 181101, Nov. 2010.
[37] P. M. Tu, C. Y. Chang, S. C. Huang, C. H. Chiu, J. R. Chang, W. T. Chang, D. S. Wuu, H. W. Zan, C. C. Lin, H. C. Kuo, and C. P. Hsu, "Investigation of efficiency droop for InGaN-based UV light-emitting diodes with InAlGaN barrier," *Appl. Phys. Lett.*, vol. 98, p. 211107, 2011.
[38] Y. K. Kuo, T. H. Wang, and J. Y. Chang, "Blue InGaN light-emitting diodes with multiple GaN-InGaN Barriers," *IEEE J. Quantum Electron.*, vol. 48, no. 7, pp. 946–951, Jul. 2012.
[39] G. Y. Liu, J. Zhang, C. K. Tan, and N. Tansu, "Efficiency-droop suppression by using large-bandgap AlGaInN thin barrier layers in InGaN quantum wells light-emitting diodes," *IEEE Photon. J.*, to be published.
[40] N. Tansu and L. J. Mawst, "Current injection efficiency of InGaAsN quantum-well lasers," *J. Appl. Phys.*, vol. 97, p. 054502, 2005.
[41] S. L. Chuang and C. S. Chang, "A band-structure model of strained quantum-well wurtzite semiconductors," *Semicond. Sci. Technol.*, vol. 12, pp. 252–263, Mar. 1997.
[42] S. L. Chuang, "Optical gain of strained wurtzite GaN quantum-well lasers," *IEEE J. Quantum Electron.*, vol. 32, pp. 1791–1800, 1996.
[43] S. L. Chuang, *Physics of Optoelectronics Devices*. Hoboken, NJ, USA: Wiley, 1995, ch. 4.
[44] H. Zhao, R. A. Arif, Y. K. Ee, and N. Tansu, "Self-consistent analysis of strain compensated InGaN-AlGaN quantum wells for lasers and light emitting diodes," *IEEE J. Quantum Electron.*, vol. 45, pp. 66–78, 2009.
[45] H. Schneider and K. V. Klitzing, "Thermionic emission and Gaussian transport of holes in a GaAs/AlGaAs As multiple-quantum-well structure," *Phys. Rev. B*, vol. 38, pp. 6160–6165, 1988.
[46] N. Tansu and L. J. Mawst, "The role of hole-leakage in 1300-nm InGaAsN quantum well lasers," *Appl. Phys. Lett.*, vol. 82, no. 10, pp. 1500–1502, Mar. 2003.
[47] I. Vurgaftman and J. R. Meyer, "Band parameters for nitrogen-containing semiconductors," *J. Appl. Phys.*, vol. 94, pp. 3675–3696, 2003.
[48] I. Vurgaftman and J. R. Meyer, *Nitride Semiconductor Devices*, J. Piprek, Ed. Hoboken, NJ, USA: Wiley, 2009, pp. 13–48.
[49] T.-S. Yeh, J.-M. Wu, and W.-H. Lan, "Electrical properties and optical bandgaps of AlInN films by reactive sputtering," *J. Crys. Growth*, vol. 310, pp. 5308–5311, 2008.
[50] M. Farahmand *et al.*, "Monte Carlo simulation of electron transport in the III-nitride wurtzite phase materials system: Binaries and ternaries," *IEEE Trans. Electron Devices*, vol. 48, pp. 535–542, 2001.
[51] P. Kozodoy, H. Xing, S. P. DenBaars, U. K. Mishra, A. Saxler, R. Perrin, S. Elhamri, and W. C. Mitchel, "Heavy doping effects in Mg-doped GaN," *J. Appl. Phys.*, vol. 87, pp. 1832–1835, 2000.
[52] Y.-C. Lu *et al.*, "Carrier trapping effects on photoluminescence decay time in InGaN/GaN quantum wells with nanocluster structures," *J. Appl. Phys.*, vol. 101, p. 063511, 2007.
[53] J. K. Son *et al.*, "Radiative and non-radiative transitions in blue quantum wells embedded in AlInGaN-based laser diodes," *Phys. Stat. Sol. (c)*, vol. 4, pp. 2780–2783, 2007.
[54] J. Hader, J. V. Moloney, B. Pasenow, S. W. Koch, M. Sabathil, N. Linder, and S. Lutgen, "On the importance of radiative and Auger losses in GaN-based quantum wells," *Appl. Phys. Lett.*, vol. 92, p. 261103, 2008.
[55] T. Mukai, M. Yamada, and S. Nakamura, "Characteristics of InGaN-based UV/blue/green/amber/red light-emitting diodes," *Jpn. J. Appl. Phys.*, vol. 38, pp. 3976–3981, 1999.
[56] M. R. Krames, O. B. Shchekin, R. Mueller-Mach, G. O. Mueller, L. Zhou, G. Harbers, and M. G. Craford, "Status and future of high-power light-emitting diodes for solid-state lighting," *J. Display Technol.*, vol. 3, no. 2, pp. 160–175, Jun. 2007.
[57] M. A. Khan, "AlGaN multiple quantum well based deep UV LEDs and their applications," *Phys. Stat. Sol. (a)*, vol. 203, pp. 1764–1770, 2006.
[58] E. Kuokstis, W. H. Sun, M. Shatalov, J. W. Yang, and M. A. Khan, "Role of alloy fluctuations in photoluminescence dynamics of AlGaN epilayers," *Appl. Phys. Lett.*, vol. 88, p. 261905, 2006.
[59] H. P. D. Schenk, M. Nemoz, M. Korytov, P. Vennegues, A. D. Drager, and A. Hangleiter, "Indium incorporation dynamics into AlInN ternary alloys for laser structures lattice matched to GaN," *Appl. Phys. Lett.*, vol. 93, p. 081116, 2008.
[60] S. Hernandez, K. Wang, D. Amabile, E. Nogales, D. Pastor, and R. Cusco, "Structural and optical properties of MOCVD InAlN epilayers," in *Mater. Res. Soc. Symp. Proc.*, 2005, vol. 892, pp. 0892–FF23.
[61] G. Liu, J. Zhang, X.-H. Li, G. S. Huang, T. Paskova, K. R. Evans, H. Zhao, and N. Tansu, "Metalorganic vapor phase epitaxy and characterizations of nearly-lattice-matched AlInN alloys on GaN/sapphire templates and free-standing GaN substrates," *J. Cryst. Growth*, vol. 340, pp. 66–73, 2012.
[62] M. H. Kim, M. F. Schubert, Q. Dai, J. K. Kim, E. F. Schubert, J. Piprek, and Y. Park, "Origin of efficiency droop in GaN-based light-emitting diodes," *Appl. Phys. Lett.*, vol. 91, no. 18, Art. 183507, Oct. 2007.
[63] A. Knauer, H. Wenzel, T. Kolbe, S. Einfeldt, M. Weyers, M. Kneissl, and G. Trankle, "Effect of the barrier composition on the polarization fields in near UV InGaN light emitting diodes," *Appl. Phys. Lett.*, vol. 92, p. 191912, 2008.
[64] C. C. Pan, S. Tanaka, F. Wu, Y. J. Zhao, J. S. Speck, S. Nakamura, S. P. DenBaars, and D. Feezell, "High-power, low-efficiency-droop semipolar (2021) single-quantum-well blue light-emitting diodes," *Appl. Phys. Exp.*, vol. 5, no. 6, Art. 062103, Jun. 2012.
[65] Y. J. Zhao, S. Tanaka, C. C. Pan, K. Fujito, D. Feezell, J. S. Speck, S. P. DenBaars, and S. Nakamura, "High-power blue-violet semipolar (2021) InGaN/GaN light-emitting diodes with low efficiency droop at 200 A/cm^2," *Appl. Phys. Exp.*, vol. 4, no. 8, Art. 082104, Aug. 2011.
[66] L. F. Xu, D. Patel, C. S. Menoni, J. Y. Yeh, L. J. Mawst, and N. Tansu, "Experimental evidence of the impact of nitrogen on carrier capture and escape times in InGaAsN/GaAs single quantum well," *IEEE Photon. J.*, vol. 4, no. 6, pp. 2262–2271, Dec. 2012.

Hongping Zhao received the Bachelor's degree in physics from Nanjing Normal University (China) in 2003, the Master's degree in electrical engineering from Southeast University (China) in 2005, and the Ph.D. degree in electrical engineering from Lehigh University, Bethlehem, PA, USA, in 2011.

Since July 2011, she has been a tenure-tracked assistant professor in the Department of Electrical Engineering and Computer Science (EECS) at Case Western Reserve University. Her research areas cover device physics, epitaxial growth, and fabrication of semiconductor optoelectronics devices based on III-nitride semiconductor nanostructures. To date, she has been author or coauthor of more than 105 research publications in refereed international journals and conference proceedings. She is a regular reviewer of the leading journals in the areas of applied physics, quantum electronics, nanotechnology, photonics and optoelectronics.

Dr. Zhao is the recipient of the SPIE educational scholarship in optical science and engineering for 2008 and 2009. She has also served as a panel review member for National Science Foundation.

Guangyu Liu received the B.S. degree in electronic science and technology from Huazhong University of Science and Technology, China, in 2008, and is currently working toward the Ph.D. degree in Department of Electrical and Computer Engineering (ECE) and Center for Photonics and Nanoelectronics at Lehigh University, Bethlehem, PA, USA.

Her research interests are related to III-Nitride semiconductor nanostructures and optoelectronics devices, covering the theoretical/computational, metalorganic chemical vapor deposition (MOCVD) growth, and device fabrication and characterization technology. The research topics include the pursuit of high-performance III-Nitride light-emitting diodes (LEDs), the growths of III-Nitride quantum dots (QDs) devices for solid state lighting and solar cells, and investigation of III-Nitride based intersubband quantum cascade laser (QCL). She has published more than 50 refereed journal and conference publications.

Ms. Liu is also a recipient of SPIE Scholarship in Optics and Photonics (Lehigh University), Sherman-Fairchild Fellowship (Lehigh University), the Dean's Scholarship (Lehigh University), and Best Graduation Thesis (Huazhong University of Science and Technology).

Jing Zhang received the B.S. degree in electronic science and technology from Huazhong University of Science and Technology, China, in 2009, and is currently working toward the Ph.D. degree in Department of Electrical and Computer Engineering (ECE) and Center for Optical Technologies (COT) at Lehigh University, Bethlehem, PA, USA.

Her research areas are related to III-Nitride semiconductor nanostructures for thermoelectric and solid state lighting technologies. Her research works cover various aspects of computational, growths, and device fabrication of III-Nitride semiconductor for photonics and thermoelectric applications. Her research topics include the pursuit of novel materials for high thermoelectric figure of merit, and solid state lighting applications.

Ms. Zhang is a recipient of the Dean's Scholarship (2009, Lehigh University), Best Graduation Thesis (2009, Huazhong University of Science and Technology), and SPIE Scholarship in Optics and Photonics (Lehigh University).

Ronald A. Arif was born in Jakarta, Indonesia, in 1980. He received the Bachelor's degree (1st class hons) in materials engineering from Nanyang Technological University (Singapore), and the Ph.D. degree in electrical engineering from Lehigh University, Bethlehem, PA, USA, in July 2008.

He worked as a Process Engineer with Agilent Technologies, Singapore from October 2002 to October 2003. He has also worked as Member of Technical Staff at EpiWorks, Inc. and Cree Inc., and is currently is a Research Scientist / Member of Technical Staff at Veeco. His research interests is related to development of high internal quantum efficiency and high performance III-Nitride LEDs and III-V lasers / solar cells by metalorganic chemical vapor deposition.

Dr. Arif has more than 50 refereed technical publications to his credit."

Nelson Tansu was born in 1977. He received the B.S. degree in applied mathematics, electrical engineering, and physics (with Highest Distinction) and the Ph.D. degree in electrical engineering/applied physics from the University of Wisconsin-Madison, Madison, WI, USA, in 1998 and 2003, respectively.

Since July 2003, he has been a faculty member in the Department of Electrical and Computer Engineering (ECE) and Center for Photonics andNanoelectronics (CPN) at Lehigh University, Bethlehem, PA, USA, where he currently is the Class of 1961 Associate Professor (with tenure). He currently serves as Associate Editor for OSA Optical Materials Express (2010–present), Assistant/ Associate Editor for Nanoscale Research Letters (2007–present), and Editor-in-Chief for Optics (2013–present). He has published in over 240 refereed international journals (92) and conference (150+) publications, and holds several U.S. patents (total > 10). He also regularly reviews leading journals in applied physics, quantum electronics, nanotechnology, photonics, and optoelectronics areas. Previously, he has given numerous lectures, seminars, and keynote and invited talks (total > 45) at universities, research institutions, and conferences in the Canada, Europe, and Asia. His research works cover both the theoretical and experimental aspects of the physics of semiconductor optoelectronics materials and devices, the physics of low-dimensional semiconductor (nanostructure), and MOCVD and device fabrications of III-Nitride and III-V-Nitride semiconductor optoelectronics devices on GaAs, InP, and GaN substrates.

Dr. Tansu served as the Primary Guest Editor of the IEEE JOURNAL OF SELECTED TOPICS IN QUANTUM ELECTRONICS (2008–2009) and IEEE/OSA JOURNAL OF DISPLAY TECHNOLOGY (2012–2013), and he also serves as an Associate Editor for IEEE PHOTONICS JOURNAL (2009–present). He served on the Technical Program Committee for several major technical conferences for IEEE, OSA, SPIE, and APS, including IEEE/OSA Conference on Lasers and Electro-Optics (2007–2009, 2013), SPIE Photonics West (2009–2013), APS March Annual Meeting (2007, 2009–2011), and ACP (2012, 2013), and others. He was selected as Invited General Participant at the 2008 National Academy of Engineering (NAE)'s U.S. Frontiers of Engineering (FOE) Symposium, and he served as the Organizing Committee for the 2009 NAE's U.S. Frontiers of Engineering Symposium. Recently, he has been invited to participate in the NAE's 2012 German-American Frontiers of Engineering Symposium (GAFOE).